Friction **10**(10): 1693–1706 (2022)
https://doi.org/10.1007/s40544-022-0601-1
ISSN 2223-7690
CN 10-1237/TH
RESEARCH ARTICLE

Mechanism of superlubricity of a DLC/Si_3N_4 contact in the presence of castor oil and other green lubricants

Yun LONG[1], Yang WANG[2,3], Volker WEIHNACHT[4], Stefan MAKOWSKI[4], Momoji KUBO[2], Jean Michel MARTIN[1], Maria-Isabel DE BARROS BOUCHET[1,*]

[1] *Ecole Centrale de Lyon, Laboratory of Tribology and System Dynamics, University of Lyon, Ecully 69134, France*

[2] *Institute for Materials Research, Tohoku University, Sendai 980-8577, Japan*

[3] *Department of Mechanical Systems Engineering, Graduate School of Engineering, Tohoku University, Sendai 980-8579, Japan*

[4] *Fraunhofer Institute for Material and Beam Technology (IWS), Dresden 01277, Germany*

Received: 03 September 2021 / Revised: 29 November 2021 / Accepted: 24 January 2022

Abstract: To meet the surging needs in energy efficiency and eco-friendly lubricants, a novel superlubricious technology using a vegetable oil and ceramic materials is proposed. By coupling different hydrogen-free amorphous carbon coatings with varying fraction of sp^2 and sp^3 hybridized carbon in presence of a commercially available silicon nitride bulk ceramic, castor oil provides superlubricity although the liquid vegetable oil film in the contact is only a few nanometres thick at most. Besides a partial liquid film possibly separating surfaces in contact, local tribochemical reactions between asperities are essential to maintain superlubricity at low speeds. High local pressure activates chemical degradation of castor oil generating graphitic/graphenic-like species on top of asperities, thus helping both the chemical polishing of surface and its chemical passivation by H and OH species. Particularly, the formation of the formation of $–(CH_2–CH_2)_n–$ noligomers have been evidenced to have a major role in the friction reduction. Computer simulation unveils that formation of chemical degradation products of castor oil on friction surfaces are favoured by the quantity of sp^2-hybridized carbon atoms in the amorphous carbon structure. Hence, tuning sp^2-carbon content in hydrogen-free amorphous carbon, in particular, on the top layers of the coating, provides an alternative way to control superlubricity achieved with castor oil and other selected green lubricants.

Keywords: superlubricity; diamond-like carbon (DLC); sp^2-hybridized carbon; hydrogen passivation; castor oil

1 Introduction

Improving the properties of lubricants and their interaction with surface material contact is an effective answer to energy crisis, resource scarcity, and global warming since good lubrication performances improve energy efficiency and prolong machinery lifetime by inhibiting friction and wear. However, for traditional mineral based oil, extra effort is required to dispose their waste and prohibit leakage of them because used oil attacks male reproductive system, causes tumours, suppresses seedlings growth, etc. [1–3]. Hence, developing more eco-friendly lubricants has been highlighted for the past 30 years.

One option in this context is to substitute traditional mineral based oils with renewable green vegetable oils. For instance, sunflower oil and soybean oil outperform mineral oil and synthetic oil by reducing 50% of friction. This is attributed to polar groups inside vegetable oils, reacting with steel surfaces and facilitating oil film growth [4], however, also contributing to poor oxidation stability [5, 6]. Other vegetable oils like coconut oil, palm oil tend to leave a larger wear scar on metallic steel ball than mineral

* Corresponding author: Maria-Isabel DE BARROS BOUCHET, E-mail: maria-isabel.de-barros@ec-lyon.fr

oil without significantly decreasing coefficient of friction (CoF) [7, 8]. Jatropha oil also causes an increase of CoF compared to mineral oil [9]. In recent years, castor oil (CO) has been reported to show very good lubricity. Quinchia et al. [10] concluded that the hydroxyl functional group makes castor oil viscous and polar, which is the main reason why castor oil overrides lubricant properties of high oleic sunflower and soybean oils. Intriguingly, under boundary lubrication, castor oil enables superlubricity of Nitinol 60 alloy/steel tribopairs, thanks to the formation of metal oxide/hydroxides layers on both surfaces. This metal oxide/hydroxide layer formation is driven by tribochemical reactions between metallic surfaces and castor oil degradation products [11]. However, superlubricity of this system vanishes when sliding speed exceeds 8 m/min [12].

More generally, some esters of glycerol could be efficient to realise superlubricity for ta-C containing tribo-pairs. For instance, with 1% of glycerol mono-oleate (GMO) in polyalphaolefin (PAO4), superlubricity is established for steel/ta-C pairs when sliding speeds are superior to 0.1 m/s [13]. Regarding glycerol (a component of vegetable oils), superlubricity is observed for self-mated ta-C pairs at 80 °C because glycerol enriches ta-C surfaces with easy sheared OH groups [14]. This superlubricity mechanism is also applicable for steel/ta-C pairs [15]. Meanwhile, the tribo-chemical interaction between Si_3N_4 and glycerol can provide superlubricity at 150 °C by forming graphenic carbon nitride nanolayers on Si_3N_4 substrate [16]. However, for steel/steel pairs, glycerol requires the help of inositol [17] or water [18] to achieve superlubricity. Being another component of vegetable oils, unsaturated fatty acids like oleic acid has already demonstrated its ability to graphitize ta-C top surfaces (less than 1 nm) and build up a pathway to superlubricity [19]. Furthermore, reactive sites of oleic acid such as C=C and COOH groups can cross-link on ta-C surfaces. Under shearing, this cross-linked oleic acid breaks, leading to defragmentation of it and surface passivation of ta-C surface [20].

Previous research of castor oil was mainly focused on metal/metal pairs. This work aims to broaden superlubricity range of castor oil by involving hydrogen-free DLC coatings and ceramic materials. Meanwhile, it provides a comparison between castor oil and conventional lubricants to improve lubricant choice for industrial application. The effect of carbon hybridization was studied by employing both sp^2-rich amorphous carbon (a-C) and sp^3-rich tetrahedral amorphous carbon (ta-C) coatings. The novel superlubricity mechanism of a-C/Si_3N_4 and ta-C/Si_3N_4 tribopairs lubricated by castor oil is investigated by comparing its performance under low sliding speed (3 mm/s) and identifying the surface chemical changes occurring after friction by X-ray photoelectron spectroscopy (XPS)/X-ray-induced Auger electron spectroscopy (XAES) surface analysis. Furthermore, comparing the coatings with different sp^2-hybridized carbon contents, it is proved that tribo-induced aromaticity is beneficial to reach the superlubricity threshold. Complementary numerical simulation results indicate that degradation products from castor oil preferentially occupy sp^2-carbon sites compared to sp^3 ones.

2 Experimental

2.1 Materials

Castor oil, glycerol (purity ≥99.5%), ricinoleic acid (purity ≥99%), oleic acid (purity ≥99%) abbreviated as CO, GL, RA, and OA are purchased from Sigma-Aldrich (St. Louis, USA). Poly-alpha-olefin 4 (PAO4) also named as Durasyn@ 164 is bought from INEOS oligomers (London, UK). Glycerol monooleate (GMO) provided by Total Energies (Paris, France) is also used in this study. Concerning tribopairs selection, coated AISI 52100 steel pins with 100 mm radius spherical head provided by Rocholl GmbH (Eschelbronn, Germany) are used to slide against Si_3N_4 flats manufactured by hot pressure sintering and provided by Lianyungang High Born Technology Co (Lianyungang, China). The hardness of steel pin is around 8 GPa. Two hydrogen-free amorphous carbon coatings with different contents of sp^2 and sp^3 hybridized carbon atoms are deposited on steel pin surfaces by Fraunhofer IWS (Dresden, Germany). The coatings were applied by pulsed laser-arc technique using a commercial physical vapour deposition (PVD) coating system, consisting of a deposition chamber

with an attached Laser-Arc™ module including a plasma-filtering unit [21]. The samples were mounted in a twofold rotation arrangement corresponding to a situation of an industrial coating of tribological components. Prior to carbon coating, Ar^+ ion etching was performed, using a hollow-cathode plasma source. After etching, a chromium interlayer with thickness of about 100 nm was deposited by magnetron sputtering. The ratio of sp^2/sp^3 carbon atoms was adjusted using different temperatures for the deposition process.

After deposition, coating thickness was measured by the ball crater method. Mechanical properties were derived from nanoindentation tests, using a ZwickRoell ZHN nanomechanical test system (Ulm, Germany). Measurements were taken with a Berkovich tip loaded up to 100 mN with quasi continuous stiffness method (QCSM). Young's modulus and hardness of the coating are acquired as described in EN ISO 14577-4:2016, however, for extrapolation of coating indentation modulus, a sigmoid fit model was used instead of the proposed linear fit. Coating Young's modulus was verified independently with surface acoustic wave spectroscopy [22], resulting in well agreeing values. Since hardness, Young's modulus, and density directly correlate with sp^3 content for hydrogen-free amorphous carbon, the ratio of sp^3 hybridized carbon F was approximated from Young's modulus E by $F = E / 800$ GPa [23].

The carbon coatings were lapped with diamond slurry to mirror finish, removing both growth defects and the native sp^2 rich top layer formed during deposition. The method to obtain surface roughness (Sa) is detailed in surface analyses section. The different properties of the virgin samples are listed in Table 1.

2.2 Friction and wear experiments

A home-made linear reciprocating tribometer with pin-on-flat configuration was used to perform sliding experiments with a movement following a sine function to vary sliding speed. The maximum speed is reached in the middle of the wear track (noted as mid-point). The tangential force is detected by a piezoelectric sensor. Before running tests, all samples were cleaned by ultra-sonication in n-heptane for 30 min then in acetone for 5 min. Before installing the pin on the flat, 50 μL of lubricants (about one droplet) was added on Si_3N_4 flats with a syringe. All tests were conducted at a temperature of 100 °C and lasted 1.1 h under a constant normal load of 50 N corresponding to an initial maximum Hertzian contact pressure of 262 MPa. Due to the large radius of curvature of DLC pins, the theoretical Hertzian contact diameter is about 600 μm. To ensure a sufficient kinematic length of sliding, the stroke length was fixed at 3 mm. Maximum sliding speeds at mid-point of 3 mm/s were used. The tangential force (F_t) and motor position are recorded every 0.001 s. The CoF of one cycle is calculated from half value of F_t difference in a round trip at mid-point. It is worthy to mention that the detection limit of CoF is 0.005 in our tribometer with a detection accuracy of ±0.001. Therefore, CoF measured below 0.005 is not representative because it is difficult to extract the signal from the noise. Furthermore, all experiments were conducted 3 times and the CoF differences among those 3 tests are within 5% of each other.

2.3 Surface and lubricant analyses

All virgin lubricants were analysed by Fourier-transform Infrared Spectroscopy (FTIR, Perkin Elmer, USA) where diamond/ZnSe crystal is used and scanning range is set up as 4,000–650 cm^{-1}.

Lubricant residues on specimens were removed by ultra-sonicating samples in n-heptane for 5 min.

Table 1 Chemical and mechanical properties of tribopair materials. The sp^3-hybridized carbon content of a-C(30) and ta-C(55) is deduced from Young's modulus. Young's modulus and hardness of the coating are measured by nanoindentation.

	Production method	Coating thickness (μm)	Sa (nm)	Indentation modulus (GPa)	$sp^3/(sp^2+sp^3)$ (%)	$sp^2/(sp^2+sp^3)$ (%)	Indentation hardness (GPa)
Si_3N_4	Hot pressing sintering	—	6.7	310	—	—	15.7
a-C(30)	Filtered laser-arc PVD	3.2	8.5	237	30	70	30
ta-C(55)	Filtered laser-arc PVD	4.0	8.1	521	65	35	55

In the following, the two different carbon coatings are named a-C(30) and ta-C(55) corresponding to their respective hardness in brackets.

Afterwards, samples were optically imaged by digital microscopy (VHX-6000, Keyence, Japan). three dimensional (3D) topographical images were recorded by interferometer (ContourGT-X, Bruker, USA). A 50× objective is used to acquire Sa. This corresponds to an area of 126 μm × 95 μm with lateral resolution of 0.2 μm. An objective with a 10 times larger measured area is also used, where curvature fitting is applied only on wear scar in order to get radius of wear scar curvature. Same fitting process is also used to acquire Sa but in an area of 126 μm × 95 μm. Surface chemistry change on samples after friction were analysed by XAES/XPS analyses with a ULVAC-PHI Versa Probe II spectrometer using Al Kα X-ray source (1,486.6 eV), a take-off angle of 45° and a probed area of 100 μm × 100 μm. In order to avoid the charge effect, a neutralization system was used and C–C/C=C contribution of C1s was indexed at a binding energy (BE) of 284.8 eV. Additionally, spectra of C1s and Auger C KLL regions were obtained with pass energy of 23.5 eV. All peaks were fitted with multipack software using Shirley background. Quantification was carried out using the transmission function of the apparatus and an angular distribution correction for 45° angle. Sensitivity factors were extracted from the Ref. [24], where cross section and escape depth correction were integrated.

The structure difference between a-C(30) and ta-C(55) materials was investigated by Raman spectroscopy using a 633 nm laser beam. Spectra were acquired on three spots, each randomly selected inside and outside of the wear scar on the coated pin. Laser power was kept approximately at 1 mW at the sample surface. By testing different laser powers, it was ensured that excitation energy was below damage threshold. After acquisition, carbon peaks are fitted within a spectral range of 900–1,900 cm^{-1} to a combined fit model consisting of a Lorentzian peak (D peak), BWF peak (G peak), and a linear base line. Fit quality was good and resulted in $R^2 > 0.993$. As parameters describing the hydrogen-free carbon structures, D/G peak ratio and G peak position are discussed as proposed by Ferrari and Robertson [25].

3 Experimental results

3.1 Influence of DLC type

First, sliding tests are conducted with a-C(30)/Si_3N_4 and ta-C(55)/Si_3N_4 friction pairs in order to explore how DLC structure influences the lubrication ability of castor oil. All the tests display a very short running-in period of duration below 15 min followed by a steady CoF below the value of 0.01 (Fig. 1(a)). This is defined as the so-called liquid superlubricity regime.

Results are very reproductible as shown for 3 consecutive tests carried out in Fig. 1(a). Interestingly, steady CoFs depend significantly on the DLC type. Here, steady CoF is accurately calculated in 2 steps: first calculating an arithmetic average value of CoFs

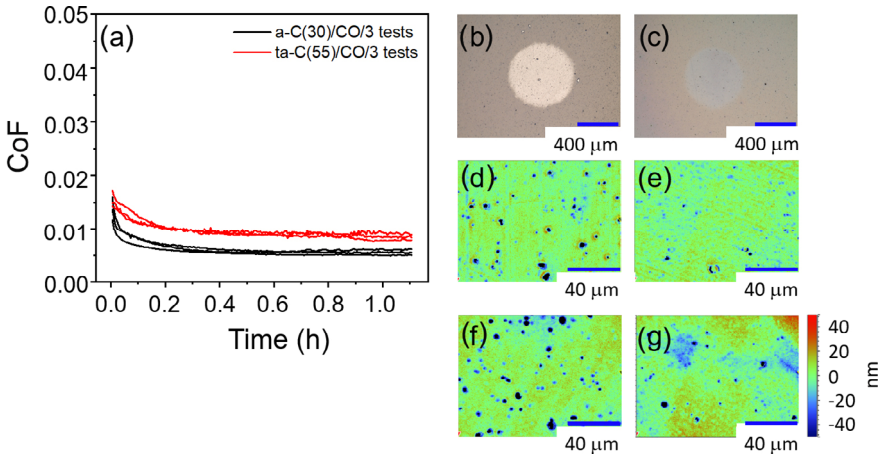

Fig. 1 Friction experiments of a-C(30)/Si_3N_4 and ta-C(55)/Si_3N_4 tribopairs lubricated by castor oil in boundary lubrication regime. (a) Friction curves at 3 mm/s; (b, c) optical images of a-C(30) pin and ta-C(55) pin wear scars; 3D profiles of a-C(30) pins (f) before and (d) after friction, ta-C(55) pins (g) before and (e) after friction. 3D profiles have been fitted with a curvature filter to direct demonstrate height distribution of surfaces.

from the last 10 min of each test; secondly taking previous values and calculating an arithmetic average of 3 repeated tests. As a result, replacing ta-C(55) by a-C(30) leads to about 30% decrease of steady CoF. The steady CoF of ta-C(55)/Si_3N_4 is 0.008 while the one of a-C(30)/Si_3N_4 is 0.0055. Value errors are below ± 0.001.

No wear track can be detected on Si_3N_4 flats by optical microscopy (Fig. S1 in the Electronic Supplementary Material (ESM)), this is rather unexpected because of the lower hardness of Si_3N_4 compared to DLC coatings. On the a-C(30) pin, a homogenous bright and circular wear scar is formed after friction test with a diameter of 650 μm (Fig. 1(b)), a value slightly larger than the Hertzian contact diameter (calculated as 600 μm). This shows a small reduction of the apparent contact pressure from 176 to 150 MPa. DLCs' local height distributions of asperities in 126 μm × 95 μm areas are shown in Figs. 1(d)–1(g). For virgin a-C(30) (Fig. 1(f)), surface is dominated by asperities with a height in the range of 10–20 nm, corresponding to orange colour. After friction, light blue colour becomes more pronounced on a-C(30) wear scar (Fig. 1(d)), indicating that asperities heights are now below 10 nm. As a consequence, the a-C(30) surface is polished reaching a Sa equal to 5.4 nm compared to original Sa of 8.5 nm for a-C(30) (Table 2). Similar results were obtained with the hardest ta-C(55) coating. No visible wear scar is observed on Si_3N_4 side in all tests and no morphological change has been recorded, either. This denies the possibility of large-scale materials transfer from DLCs side to Si_3N_4. However, this similarity doesn't explain why the CoF of a-C(30) stabilizes at 0.0055 while the steady CoF of ta-C(55) is significantly higher at 0.008. It is interesting to notice that the wear scar on the pin is not completely truncated but that the radius of curvature inside the scar is a little bit larger than 100 μm inducing a very low wear volume < 4,000 μm^3. And the wear depth of a-C is around 25 nm while the wear depth of ta-C is 10 nm. This is included in the calculation of film thickness.

Table 2 Comparison of DLC wear status and their lubrication regime in castor oil. The calculations of liquid film thickness and theoretical CoF of Couette flow are detailed in the ESM.

DLC(x)/Si_3N_4	a-C(30)	ta-C(55)
Steady-state CoF	0.005	0.008
Theoretical CoF considering Couette flow	0.0005	0.0005
Wear scar diameter (mm)	0.62	0.63
Radius of curvature inside the wear scar (mm)	125	105
Apparent contact pressure (MPa)	148	170
Roughness Sa before test (nm)	8.5	8.1
Roughness Sa after test (nm)	5.4	5.4
Oil film thickness before test (nm)	3.5	3.5
Lambda before test	0.30	0.31
Film thickness after test (nm)	3.9	3.5
Lambda after test	0.40	0.36

The question is which lubrification regime is at work in our conditions. We performed elastohydrodynamic lubrication (EHL) calculations to determine the theoretical minimum film thickness for both cases. Because of the low roughness inside the wear scar, a fluid film could support the load and could give low friction. Also, we calculated the theoretical CoF considering Couette flow and infinitely smooth surfaces (detailed in the ESM: Theoretical CoF arisen from liquid) in the contact area. As shown in Table 2, lambda value is inferior to 1 both before and after shearing. This indicates friction tests are conducted in boundary lubrication.

First, we assume that the wear and polishing mechanism on the pin take place during the running-in period where friction is higher. The calculated film thickness is about 5 nm in both cases corresponding to a lambda value below unity (typical of boundary lubrication) and Couette friction associated is much lower than 0.01. In the literature it is generally accepted that EHL is not at work when the film thickness is below 5 nm. Moreover, in our case, castor oil is a relatively large molecule with a non-planar 3-D configuration providing a pressure-viscosity coefficient above 10 GPa^{-1}. The spherical average size of the molecule in the liquid can be estimated between 3 and 4 nm (at least twice the length of the ricinoleic acid). In these conditions the gap of 5 nm in the contact does not permit the molecules to slide easily on each like in a liquid and the definition of viscosity in this kind of interface is more than questionable so that we can confirm that the EHL standard calculation cannot apply in our case. It is more probable that the molecule is quickly decomposed

under shear stress as we will see in the atomistic calculations. Then the superlubricity regime is more dominated by surface chemistry than by oil viscosity parameters.

To reveal underlying chemical mechanism, XPS/XAES analysis is used to investigate surface chemistry changes inside and outside of wear scars for DLC pins. As we already mentioned, Si_3N_4 flats could not be analysed because the wear scar is not detectable by optical microscopy, so only DLC pin counterparts are analysed after friction.

Due to lack of characteristic peaks other that of carbon and oxygen, spectra are calibrated for all samples by fixing the C1s photopeak at the same BE of 284.8 eV corresponding to C–C/C–H chemical bonds. Obviously the full width at half maximum (FWHM) of C–C/C=C peak inside wear scar is significantly larger than outside (Fig. 2, Table 3) regardless of the DLC type.

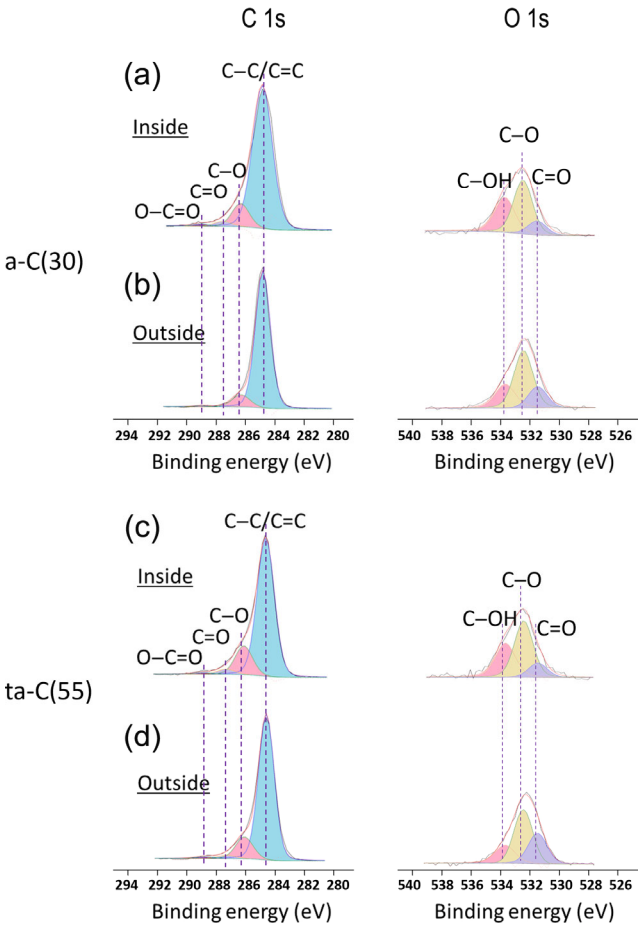

Fig. 2 C 1s and O 1s XPS spectra of DLC pins after testing where (a, c) recorded inside of wear scar for a-C(30) and ta-C(55) while (b, d) are recorded outside of wear scar for a-C(30) and ta-C(55).

This strongly suggests that a significant part of sp^2 carbon is formed inside the wear scar and has been produced by the tribochemical reactions.

Moreover, by comparing outside and inside of wear scars, stronger contributions of C–O, C=O, and O–C=O (peaking at 286.3, 287.5, and 289.0 eV, respectively) as well as C–OH on the O 1s photopeak are found inside of wear scar. In particular, the increase of C–OH content inside wear scar is compared with outside: a-C(30) shows an increase of 11% of C–O while ta-C(55) exhibits 14% increase. This oxygen content increases inside DLC wear scars could originate from the chemical reaction of castor oil (or its degradation products) with DLC material.

Since the change in sp^2 carbon content before and after friction cannot be deduced accurately from the fitting of the XPS C1s peak, we investigated the Auger C KLL first-derivative signal in the XPS spectra (so-called XAES) to identify more accurately the hybridization state and chemical bonding of carbon on DLC surface.

In Fig. 3, we measured the distance between the highest and the lowest kinetic energies that is known as the *D* parameter [26] A linear relationship is often accepted between *D* parameter and sp^2/sp^3 ratio on a carbon surface [27]. Our results show that a larger *D* parameter is always observed inside wear scar compared to outside, and this for both type of DLC. The *D* parameters of a-C(30), ta-C(55) wear scar are 18.4, 16.4 eV, respectively. Knowing that *D* parameter of graphite is 20 eV and *D* parameter of diamond is 14.2 eV [28], a 2 eV difference between a-C(30) and ta-C(55) wear scars means 24% difference for sp^2 content. The sp^2 content of a-C(30) wear scar reaches 71%. This enrichment in sp^2 carbon is located at the extreme surface of the wear scar since the Auger C KLL signal comes from a depth of only 1.5 nm compared with the C 1s signal originating from 5 nm depth (in the ESM: XPS information depth calculation).

Interestingly, an additional peak at 261.5 eV clearly appears between the highest and the lowest energies inside a-C(30) wear scar showing the lowest friction coefficient. Such extra peak shows up while analysing pure polyethylene (PE) but not in polystyrene (PS) and polyacetylene (PA) (Fig. 3) [29]. This peak also exists in DLC coatings which are fabricated by adopting

Table 3 Fitting details of Fig. 2.

	C 1s					O 1s	
	C–C/C=C	C–O	C=O	O–C=O	C–OH	C–O	C=O
BE (eV)	284.8	286.3	287.5	290.0	533.7	532.4	531.5
a-C(30) inside wear scar							
FWHM (eV)	1.6	1.4	1.4	1.2	1.6	1.5	1.5
Content (%)	84.3	12.0	2.6	1.1	36.7	51.2	12.1
a-C(30) outside wear scar							
FWHM (eV)	1.2	1.4	1.4	1.2	1.6	1.5	1.5
Content (%)	90.0	9.4	—	0.6	25.2	55.5	19.3
ta-C(55) inside wear scar							
FWHM (eV)	1.4	1.4	1.4	1.4	1.6	1.5	1.5
Content (%)	79.2	16.7	3.1	1.0	34.9	51.8	13.3
ta-C(55) outside wear scar							
FWHM (eV)	1.2	1.4	1.4	1.4	1.6	1.5	1.5
Content (%)	83.0	13.8	2.1	1.1	20.2	49.0	30.8

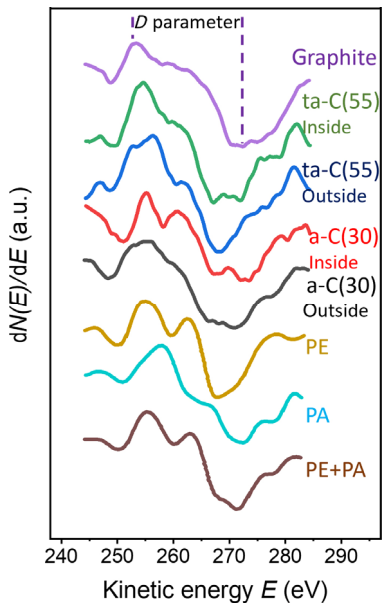

Fig. 3 Comparison of the first derivation of XAES CKLL spectra performed inside (red) and outside (black) wear track of a-C(30), inside (green) and outside (blue) wear track of ta-C(55), graphite (violet), polyethylene-PE (light brown), polyacetylene-PA (cyan), and mixture of PE and PA (dark brown). The spectra for PA–PE, PE, and PA are reproduced. Reproduced with permission from Ref. [29], © American Chemical Society, 2018.

CH=CH as precursor but not in those coatings produced by using CH_4 and C_6H_6 [30]. And it has been recently remarked after friction test of hydrogenated DLC (a-C:H) in vacuum and attributed to $–(CH_2–CH_2)_n–$ oligomers in agreement with atomistic calculations [31]. Hence, XAES data indicates that $–(CH_2–CH_2)_n–$ oligomers are present on a-C(30) wear scar. It is worthy to highlight that PE+PA mixture also owns this peak. So the existence of alkene groups on a-C(30) surface can't be excluded. Here, both a-C(30) and ta-C(55) are hydrogen-free DLC and therefore, the source of $–(CH_2–CH_2)_n–$ oligomers formation on DLC is certainly castor oil degradation. This is consistent with the fact that no clear peak at 261.5 eV is detected outside of wear scar.

Summarizing our analytical data, the top surface of a-C(30) is found to be polished after shearing, enriched in sp^2 carbon and partially terminated by some hydroxyl groups and mostly alkene and alkane groups. This situation is typically favourable for giving a very low shear strength offering an efficient pathway to limit the energy dissipation at the top of asperities [32].

3.2 Results with other green lubricants

Lubrication of DLC/Si_3N_4 pair is investigated with some other interesting green lubricants: glycerol monooleate (GMO), Glycerol, oleic acid, ricinoleic acid, and PAO4 synthetic base oil. When analysed by infrared spectrometer, GMO, glycerol, ricinoleic acid, and castor oil show wide OH stretching vibration in

between 3,000–3,650 cm^{-1} while oleic acid and ricinoleic acid show a broad band in the region 2,500–3,300 cm^{-1} which features OH stretching of carboxylic acid functions [33]. As expected, no OH stretch has been observed for PAO4 (Fig. 4(d)). Interestingly, by sliding a-C(30)/Si_3N_4 under the identical experimental conditions, superlubricity is only observed for GMO, glycerol, ricinoleic acid, and castor oil containing OH groups bonded with CH or CH_2 (Fig. 4(a)). As for oleic acid, its OH function only exists in carboxylic group and final CoF is recorded as 0.012 at 1.1 h. Summarising, a higher CoF shows up when no OH group is present in lubricants like PAO4. This observation is consistent with the fact that OH groups benefits friction reduction as already reported elsewhere [12]. It is worthy to note that under the same conditions, a-C(30) shows a lower friction coefficient than ta-C(55) while sliding in ricinoleic acid (Fig. 4(b)). A higher *D* parameter in the Auger peak derivative is detected on a-C(30) wear scar comparing with the one of ta-C(55) (Fig. S2 in the ESM). Accompanying the enlargement of *D* parameter, a significant peak at 261.5 eV is also observed for a-C(30) wear scars under lubrication by GMO and CO where superlubricity is reached (CoF << 0.01). At the opposite, the peak is weaker for RA (CoF about 0.01) and outside wear scar in all cases. This shows that CH_x-termination plays a key role in the superlow friction achievement.

Raman spectra of a-C(30) and ta-C(55) coatings inside and outside the wear track were analysed regarding G peak position and D/G peak height ratio, and results are shown in Fig. 4(c). No noteworthy D peak is found for ta-C(55) which is typical of super hard coatings, indicating a fully amorphous sp^3-rich carbon network [25]. After sliding, the structure is unchanged and no D peak appeared, still indicating a fully amorphous structure. Only a very small shift of the G peak to lower wavenumbers is observed, which could be attributed to intrinsic stress relaxation [34] or minor sp^3 to sp^2 rehybridization.

In contrast, a-C(30) shows a distinct D shoulder in the initial state, commonly found for a-C coatings deposited with high deposition rates or elevated deposition temperature. The fraction of the rigid

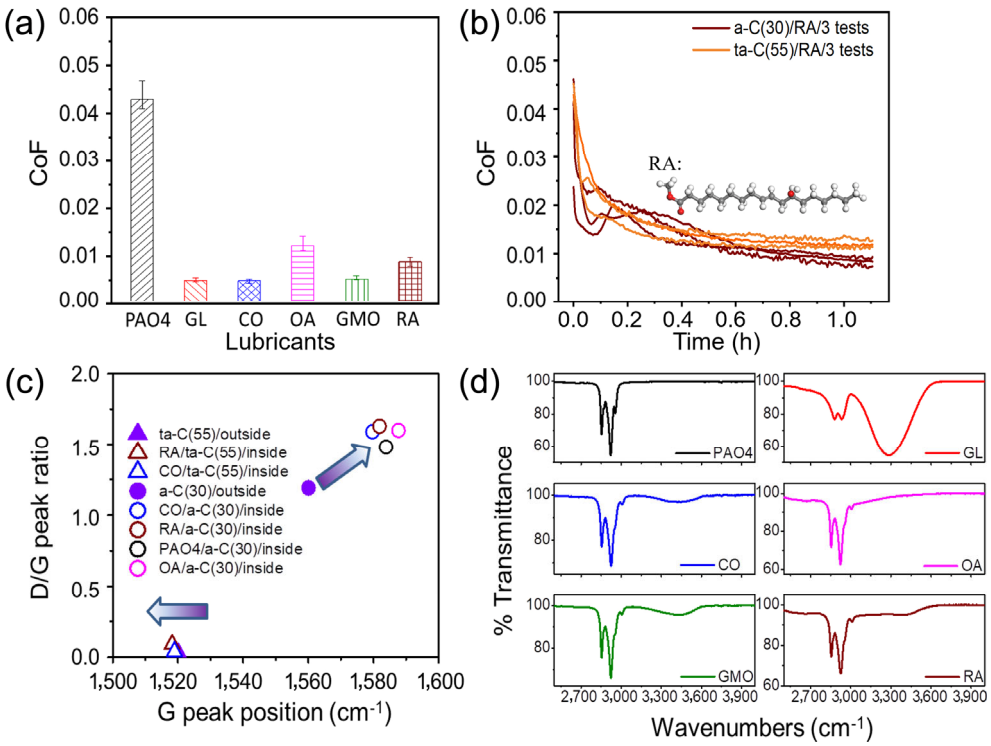

Fig. 4 (a) Final CoFs for a-C(30)/Si_3N_4 lubricated by different lubricants at 100 °C, 3 mm/s; (b) friction curves of both a-C(30)/Si_3N_4 and ta-C(55)/Si_3N_4 lubricated by RA under the same conditions. The inset image represents the molecular structure of RA with carbon in grey, oxygen in red, and hydrogen in white spheres. (c) D and G peaks information acquired from Raman spectrums, where arrows indicate change from initial surface (outside) to wear scar (inside); and (d) FTIR spectra of different lubricants.

network of sp^3 carbon is much smaller, leaving sp^2 carbon atoms enough space to rearrange and increasing order during or after deposition. As expected, the initial a-C(30) structure comprises some amorphous sp^3 carbon network, some amorphous sp^2 network and some nano-clustered sp^2 sites, which are responsible for the shoulder at the D peak position. After sliding, the D peak has increased and the G peak has shifted to higher wave numbers, resulting from an increase in structured sp^2 sites. It can be seen that such increase of sp^2 nanocluster took place with all lubricants with a-C(30), regardless of the friction level. This is in contrast with ta-C(55), where no initial sp^2 nanoclusters were present and also did not develop during sliding. Since Raman spectroscopy is probing to a depth of 1 μm, much deeper from the surface than XAES, the sp^2 ordering process resulting from sliding is likely a mechanical, shear-induced process [20].

In brief, both Raman and XAES confirm that a-C(30) with initial nano-clustered sp^2 sites are easier to realise sp^2 ordering under shearing than ta-C(55). And since low friction behaviours of a-C(30)/Si_3N_4 is also influenced by lubricants. The way how castor oil participate tribo-chemical reaction is further elucidated by simulation.

4 Atomistic simulation

To understand what happens at the real contact asperities and clarify the mechanisms of superlubricity, atomistic simulations are performed based on the molecular dynamics (MD) simulation approach with a reactive force field (ReaxFF) [35]. The ReaxFF parameter set for hydrocarbon system was reported elsewhere [36]. It was developed based on the parameter set of $ReaxFF_{C2013}$ [37] and has been proved to be able to describe the mechanical properties of solid-state carbon materials very well by comparing with first-principle calculations and experiments [38, 39]. As shown in Fig. 5, a Si_3N_4 upper slab slides against a bottom ta-C (50% sp^3) slab in the presence of RA molecules. For simulations, castor oil can be simplified to be the triglyceride species formed from ricinoleic acid and glycerol. Hence the reactions of ricinoleic acid and castor oil with the surfaces should be very similar. Moreover, as shown before, both glycerol and ricinoleic acid provide superlow friction in tribological tests. The molecular structure of ricinoleic acid is shown below the simulation model in Fig. 5. For both Si_3N_4 and ta-C, the surfaces are fully terminated by hydrogen terminations and have the same sinusoidal shape with a height of 1 nm. During the friction simulation, atoms in the top layer of upper Si_3N_4 substrate are kept rigid and forcibly slid along x-direction with a speed of 100 m/s. Meanwhile, a normal pressure of 10 GPa is applied to the rigid layer. Atoms in the bottom layer of lower ta-C substrate are also kept rigid and stationary during the whole friction simulation. The layers neighbouring to the rigid layers are thermostat layers, which means, temperature of the thermostat layers is always controlled at 300 K during the simulation. Velocity–Verlet algorithm is used to calculate the motion of each atom in the simulation system with a time step of 0.25 fs/step. The friction simulation is performed for totally 150 ps. In these simulations, we did not measure the friction force.

Figure 6 shows the snapshots of friction simulation of Si_3N_4 against ta-C. From the snapshots, even though we observe a slight elastic deformation of Si_3N_4 during the sliding (Figs. 6(b) and 6(c)), there is no visible damage of both Si_3N_4 and ta-C surfaces after 150 ps of friction. Then, to obtain clear insights into the reactions between ricinoleic acid molecules and surfaces and then compare with experimental observations, the upper Si_3N_4 substrate is uplifted after the friction (Fig. 6(d)). We clearly confirm the tribochemical

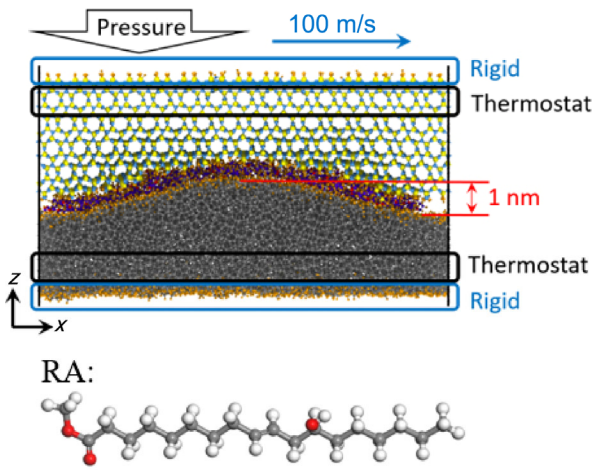

Fig. 5 Simulation model of the Si_3N_4/ta-C friction pair. Ricinoleic acid molecules are between two substrates.

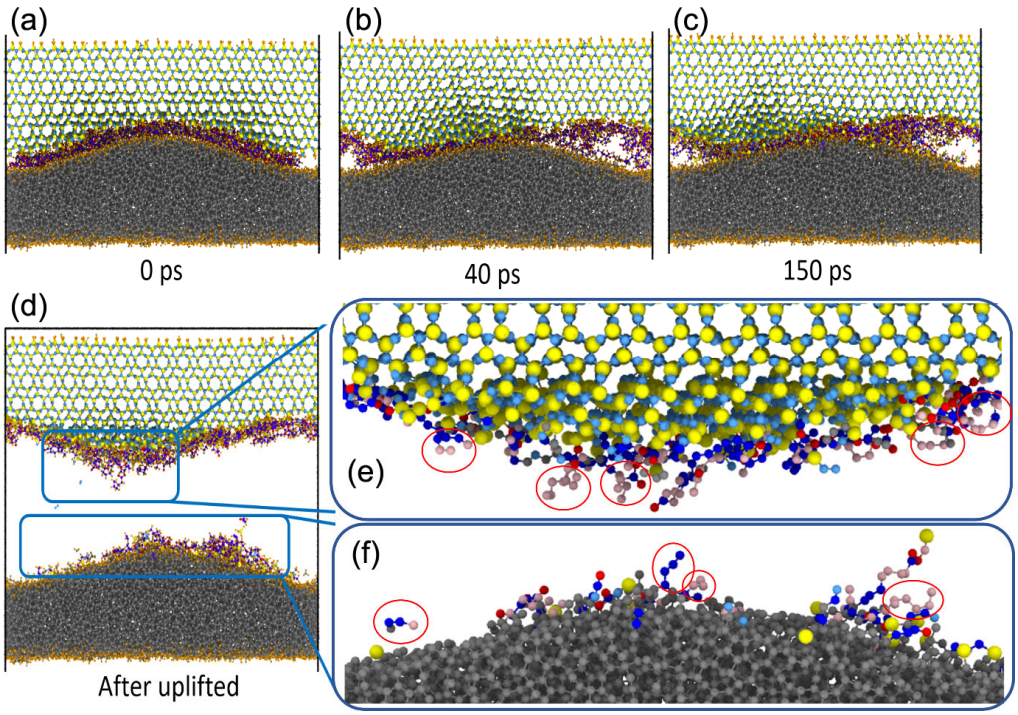

Fig. 6 Snapshots of friction simulation of Si_3N_4 against ta-C lubricated by ricinoleic acid molecules. (a) Initial state; (b) at 40 ps; (c) at 150 ps; and (d) uplifted after 150 ps. (e) and (f) are magnifications of the Si_3N_4 and ta-C surfaces respectively in (d), where in (e, f), hydrogen atoms as well as the small gas-phase molecules that do not bond to either Si_3N_4 or ta-C substrates have been hidden for clarity, while the colour of sp^2 and sp^3 type carbon in oil are assigned to dark blue and rose respectively to visualize the distributions of carbon atoms on surfaces. Alkanes and alkenes groups have been highlighted by red cycles.

reaction of ricinoleic acid molecules on both Si_3N_4 and ta-C surfaces, agreeing with the experimental observations and chemical analyses (Fig. 2). On the Si_3N_4 side, the oil adsorption occurs accompanied with the surface amorphization. Alkane, alkene, and some OH terminations are visible (Figs. 6(e) and 6(f)). Then we investigate the distribution of sp^2 and sp^3 type carbon atoms that move from the oil to Si_3N_4 and ta-C surface, as shown in Figs. 6(e) and 6(f) respectively where hydrogen atoms and the small gas-phase molecules that do not bond to either Si_3N_4 or ta-C substrates are invisible for clarity. In Figs. 6(e) and 6(f), although each RA molecule has only one alkene group (C=C bond), both Si3N4 and ta-C surfaces contain a plenty of sp^2 type carbon atoms perhaps owing to the decomposition and dehydration of RA molecules. On the Si_3N_4 surface, it is interesting to observe that sp^2 type carbon atoms are much closer to the surface than sp^3 type ones, indicating the higher reactivity of sp^2 type carbon. While on the ta-C surface, the amounts of sp^3 and sp^2 type carbon atoms are almost identical. We further focus on the unabsorbed molecules after friction. Figure 7 shows some typical unabsorbed molecules remaining in the simulation cell, which mainly includes alkanes, aldehydes, alcohols, and other complex small molecules. All of them were originally a part of ricinoleic acids. These results indicate a decomposition of ricinoleic acid molecule during the friction, highlighting the critical role of the contact pressure and shear between the asperities on the initiation of tribochemical reactions.

Based on above simulation results, the tribochemical reactions regarding ricinoleic acid at the friction interface of Si_3N_4/ta-C can be concluded as following: the ricinoleic acid molecules trapped between asperities are firstly decomposed into various small active molecule fragments under shearing, and then a part of these small molecules is attached to the ta-C surfaces forming a chemisorbed layer. Considering the above experiments in which solid contact between surface asperities exist and make a large contribution to the overall friction, this adsorbed layer on the asperity surface can effectively prevent this solid contact of asperities and hence decrease the friction

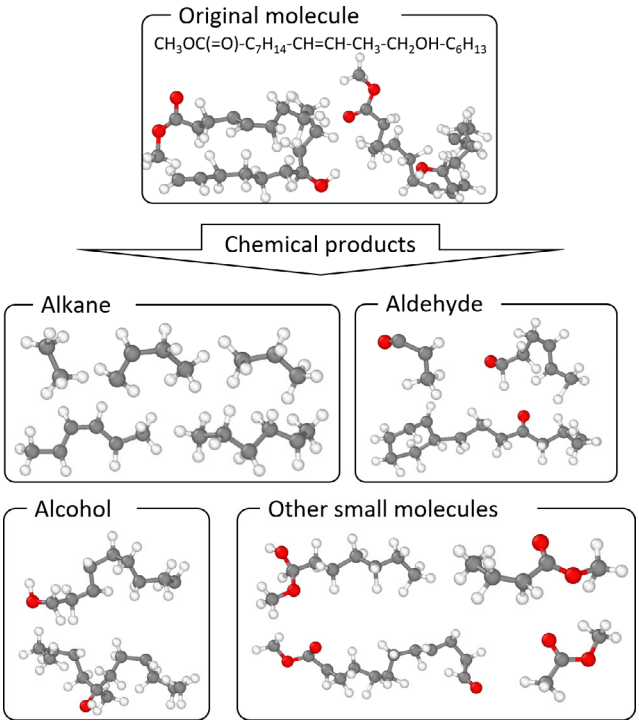

Fig. 7 Typical decomposition products of ricinoleic acid after friction. Here white, grey, and red indicate hydrogen, carbon, and oxygen, respectively.

force of the solid contact region, acting as the origin of superlubricity in experiments.

Next, to understand the difference in frictional behaviour observed in the presence of castor oil between the materials a-C(30) and ta-C(55) in the experiments, we investigate which kind of hybridized carbon atoms (sp, sp^2, or sp^3) on ta-C surface is preferred to react with ricinoleic acid. Figure 8(a) shows the percentage of each hybridization states that are preferentially bonded to ricinoleic acid fragments. For the reacted carbon, sp, sp^2, and sp^3-hybridized carbon atoms are 3.29%, 55.26%, and 41.45%, respectively, indicating that ricinoleic acid clearly preferentially reacts with sp^2-hybridized carbon atoms compared to sp^3-ones. Moreover, the evolution of hybridization ratio after friction for a ta-C material with an initial sp^2 ratio around 50% is displayed by the comparison between Figs. 8(b) and 8(c). The amounts of sp and sp^2- hybridized carbon (0.37% and 51.07%, respectively) are higher after friction than the original amounts in ta-C (0.19% and 49.16%, respectively). On the opposite, the sp^3-hybridized carbon atoms decrease from 50.64% to only 48.56% after friction (only a few tens ps). Above results indicate that ricinoleic acid fragments are more likely to react with sp and sp^2-hybridized carbons. In addition, it was observed that the sp and sp^2 amounts in ta-C increased slightly after friction while the sp^3 ratio decreased (comparison of Figs. 8(b) and 8(c)). This tendency to re-hybridize in the sp and sp^2 states helps to reduce friction by providing more active adsorption sites. The result of the simulation is consistent with our experiments (Figs. 2 and 3). For the a-C(30) sample, even though there is no significant change in the amount of surface asperities in real contact compared with ta-C(55) due to the similar surface roughness, the higher sp^2-carbon amount in ta-C(30) sample and its ability to form more structured sp^2 sites make the surface more likely to react with the castor oil molecules, improving the formation of the adsorbed oil layer and preventing direct solid contact between ta-C and Si_3N_4.

5 Discussions

In both CO and RA, a-C/Si_3N_4 tribo-pair is preferred than ta-C/Si_3N_4 in terms of friction reduction. Moreover, replacing ta-C/Si_3N_4 by a-C/Si_3N_4 further decrease CoF is observed reaching the superlubricity regime. Such reduction of CoF originates from high initial sp^2

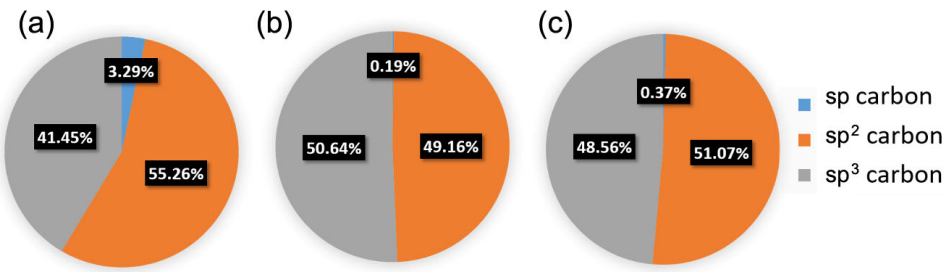

Fig. 8 Percentage of each kind of hybridized carbon atoms in simulations. (a) Carbon atoms that are bonded with ricinoleic acid fragments; (b) and (c) carbon atoms in ta-C before and after friction, respectively.

carbon content of a-C comparing with ta-C. It not only facilitates the sp^2 ordering on DLC surfaces but also influences oil molecules chemisorption on DLC surfaces because sp^2 carbon is usually more reactive than sp^3 carbon (Fig. 8).

However, oil molecules don't stay intact in the contact, undergoing a cascade of chemical decomposition into small fragments (Fig. 7) covering both DLC and Si_3N_4. Among all these fragments, mixed chains of alkane and alkene play a major role and they are also found by simulation. The existence of alkane and alkene groups on a-C after friction test is demonstrated by XAES analysis (Fig. 3). Interestingly, RA molecule has only one alkene group. So, the formation of alkene chains is most likely due to dehydration of alkane chains under shearing. These alkane and alkene chains passivate both surfaces and support partially the load and avoid direct contact between asperities [40].

On the other hand, by comparing tribological performance of a-C/Si_3N_4 in different lubricants, those with OH functions are preferred to minimize CoF. Their advantage derives from two aspects: firstly, OH function serves as anchoring spot to bridge oil molecule and surfaces [20]; secondly, the OH function helps for surface hydroxylation. DLC surfaces passivated by OH functions have been always associated with low friction in previous works [41, 12]. However, in our case, CH_x-termination (by both alkanes and alkenes) is the dominant mechanism because the characteristic CH_2 feature at 261.5 eV in the Auger CKLL peak is more intense when friction is low and this independently of the oxygen content of the lubricant (see the case of GMO for example in Fig. S2 in the ESM).

6 Conclusions

This study enlarges the potential application range of castor oil as a superlubricant under boundary lubrication. Previously evidenced for nickel alloys, it is here enlarged to Si_3N_4 ceramics and H-free DLC (a-C or ta-C), a highly wear-resistant tribopair, and this even under severe boundary lubrication conditions (low speed and lambda ratio <1). This green superlubricity mechanism is enabled by mitigating the shear strength at the level of asperities by the tribo-induced formation of graphitic/graphenic nanolayers, surface hydroxylation, and $-(CH_2–CH_2)_n-$ oligomers on surface. Such mechanism preferentially occurs on sp^2-rich amorphous carbon coatings, initially containing some nano-clustered graphite sites such as a-C(30). The importance of carbon re-hybridization process from sp^3 to sp^2 on the chemical adsorption and reaction of the castor oil molecular fragments is highlighted using atomistic calculation and additional action on the flattening top surface of asperities at a nano-scale could be expected. Thus, through tailoring initial sp^2-hybridized carbon content at the ta-C surface, friction can be governed.

Acknowledgements

This research is supported by TOTAL, Solaize Research Center and Federal Ministry of Economic Affairs and Energy Germany (BMWi) within project CHEOPS3 (Funding number 03ET1286B). The authors wish to express their acknowledgement to the Agence Nationale de la Recherche (ANR) for partial funding of ULVAC-PHI Versa Probe II XPS spectrometer.

Electronic Supplementary Material: Supplementary material is available in the online version of this article at https://doi.org/10.1007/s40544-022-0601-1.

References

[1] Akintunde W O, Olugbenga O A, Olufemi O O. Some adverse effects of used engine oil (common waste pollutant) on reproduction of male sprague dawley rats. *Maced J Med Sci* **3**(1): 46 (2015)

[2] Grimmer G, Dettbarn G, Brune H, Deutsch-Wenzel R, Misfeld J. Quantification of the carcinogenic effect of polycyclic aromatic hydrocarbons in used engine oil by topical application onto the skin of mice. *Int Arch Occup Environ Health* **50**(1): 95–100 (1982)

[3] Kayode J, Olowoyo O, Oyedeji A. The effects of used engine oil pollution on the growth and early seedling performance of vigna uniguiculata and zea mays. *Res J Soil Biol* **1**(1): 15–19 (2009)

[4] Alves S M, Barros B S, Trajano M F, Ribeiro K S B, Moura E J T I. Tribological behavior of vegetable oil-based lubricants with nanoparticles of oxides in boundary lubrication conditions. *Tribol Int* **65**: 28–36 (2013)

[5] Wagner H, Luther R, Mang T. Lubricant base fluids based on renewable raw materials. *Appl Catal A* **221**(1–2): 429–442 (2001)

[6] Fox N J, Stachowiak G W. Vegetable oil-based lubricants—A review of oxidation. *Tribol Int* **40**(7): 1035–1046 (2007)

[7] Jayadas N H, Nair K P, Ajithkumar G. Tribological evaluation of coconut oil as an environment-friendly lubricant. *Tribol int* **40**(2): 350–354 (2007)

[8] Masjuki H H, Maleque M A, Kubo A, Nonaka T. Palm oil and mineral oil based lubricants—Their tribological and emission performance. *Tribol Int* **32**(6): 305–314 (1999)

[9] Syahrullail S, Kamitani S, Shakirin A J P E. Performance of vegetable oil as lubricant in extreme pressure condition. *Procedia Eng* **68**: 172–177 (2013)

[10] Quinchia L A, Delgado M A, Reddyhoff T, Gallegos C, Spikes H A. Tribological studies of potential vegetable oil-based lubricants containing environmentally friendly viscosity modifiers. *Tribol Int* **69**: 110–117 (2014)

[11] Zeng Q, Dong G, Martin J M. Green superlubricity of nitinol 60 alloy against steel in presence of castor oil. *Sci Rep* **6**(1): 29992 (2016)

[12] Zeng Q, Dong G. Influence of load and sliding speed on super-low friction of nitinol 60 alloy under castor oil lubrication. *Tribol Lett* **52**(1): 47–55 (2013)

[13] Kano M. Super low friction of DLC applied to engine cam follower lubricated with ester-containing oil. *Tribol Int* **39**(12): 1682–1685 (2006)

[14] Bouchet M I D B, Matta C, Le-Mogne T, Martin J M, Zhang, Q, Goddard III W, Kano M, Mabuchi Y, Ye J. Superlubricity mechanism of diamond-like carbon with glycerol: Coupling of experimental and simulation studies. *J Phy Conf Ser* **89**(1): 012003 (2007).

[15] Long Y, Bouchet M I D B, Lubrecht T, Onodera T, Martin J M. Superlubricity of glycerol by self-sustained chemical polishing. *Sci Rep* **9**(1): 6286 (2019)

[16] Long Y, Kuwahara T, Bouchet M I D B, Ristić A, Dörr N, Lubrecht T, Dupuy L, Moras G, Martin J M, Moseler M. *In situ* synthesis of graphene nitride nanolayers on glycerol-lubricated Si3N4 for superlubricity applications. *ACS Appl Nano Mater* **4**(3): 2721–2732 (2021)

[17] Matta C, Joly-Pottuz L, Bouchet M I D B, Martin J M, Kano M, Zhang Q, Goddard III W A. Superlubricity and tribochemistry of polyhydric alcohols. *Phys Rev B* **78**(8): 085436 (2008)

[18] Chen Z, Liu Y, Zhang S, Luo J. Controllable superlubricity of glycerol solution via environment humidity. *Langmuir* **29**(38): 11924–11930 (2013)

[19] Bouchet M I D B, Martin J M, Avila J, Kano M, Yoshida K, Tsuruda T, Shandan B, Yuji H, Nobuki O, Momoji K, Asensio M C. Diamond-like carbon coating under oleic acid lubrication: Evidence for graphene oxide formation in superlow friction. *Sci Rep* **7**(1): 46394 (2017)

[20] Kuwahara T, Romero P A, Makowski S, Weihnacht V, Moras G, Moseler M. Mechano-chemical decomposition of organic friction modifiers with multiple reactive centres induces superlubricity of ta-C. *Nat Com* **10**(1): 151 (2019)

[21] Kaulfuss F, Weihnacht V, Zawischa M, Lorenz L, Makowski S, Hofmann F, Leson A. Effect of energy and temperature on tetrahedral amorphous carbon coatings deposited by filtered laser-arc. *Materials* **14**: 2176 (2021)

[22] Schneider D, Schwarz T, Scheibe H J, Panzner M. Non-destructive evaluation of diamond and diamond-like carbon films by laser induced surface acoustic waves. *Thin Solid Films* **295**(1–2): 107–116 (1997)

[23] Schultrich B. *Tetrahedrally bonded amorphous carbon films I: Basics, structure and preparation.* New York (USA): Springer, 2018.

[24] Wagner C D, Davis L E, Zeller M V, Taylor J A, Raymond R H, Gale L H. Empirical atomic sensitivity factors for quantitative analysis by electron spectroscopy for chemical analysis. *Surf Interface Anal* **3**(5): 211–225 (1981)

[25] Ferrari A C, Robertson J. Interpretation of Raman spectra of disordered and amorphous carbon. *Phys Rev B* **61**(20): 14095 (2000)

[26] Lascovich J C, Scaglione S. Comparison among XAES, PELS and XPS techniques for evaluation of sp^2 percentage in aC: H. *Appl Surf Sci* **78**(1): 17–23 (1994)

[27] Kaciulis S. Spectroscopy of carbon: From diamond to nitride films. *Surf Interface Anal* **44**(8): 1155–1161 (2012)

[28] Lascovich J C. Giorgi R. Scaglione S. Evaluation of the sp^2/sp^3 ratio in amorphous carbon structure by XPS and XAES. *Appl Surf Sci* **47**: 17–21 (1991)

[29] Lee S Y, Lyu J, Kang S, Lu S J, Bielawski C W. Ascertaining the carbon hybridization states of synthetic polymers with X-ray induced Auger electron spectroscopy. *J Phys Chem C* **122**(22): 11855–11861 (2018)

[30] Sarangi D, Panwar O S, Kumar S, Bhattacharyya R. Characterization studies of diamond-like carbon films grown using a saddle-field fast-atom-beam source. *J Vac Sci Technol A* **18**(5): 2302–2311 (2000)

[31] Kuwahara T, Long Y, Bouchet M I D B, Martin J M, Moras G, Moseler M. Superlow friction of a-C:H coatings in vacuum: passivation regimes and structural characterization of the sliding interfaces. *Coatings* **11**(9): 1069 (2021)

[32] Chen X, Zhang C, Kato T, Yang X A, Wu S, Wang R, Masataka N, Luo J. Evolution of tribo-induced interfacial nanostructures governing superlubricity in aC: H and aC: H: Si films. *Nat Com* **8**(1): 1675 (2017)

[33] Kowalik P, Elbaum D, Mikulski J, Fronc K, Kamińska I, Morais P C, De Souza P E, Nunes R B, Veiga-Souza F H, Gruzeł G, Minikayev R. Upconversion fluorescence imaging of HeLa cells using ROS generating SiO_2-coated lanthanide-doped $NaYF_4$ nanoconstructs. *RSC Adv* **7**(48): 30262–30273 (2017)

[34] Ager III J W, Anders S, Anders A, Brown I G. Effect of intrinsic growth stress on the Raman spectra of vacuum–arc–deposited amorphous carbon films. *Appl Phys Lett* **66**(25): 3444–3446 (1995)

[35] Van Duin A C, Dasgupta S, Lorant F, Goddard W A. ReaxFF: A reactive force field for hydrocarbons. *J Phys Chem A* **105**(41): 9396–9409 (2001)

[36] Wang Y, Shi Y, Sun Q, Lu K, Kubo M, Xu J. Development of a transferable ReaxFF parameter set for carbon and silicon-based solid systems. *J Phys Chem C* **124**(18): 10007–10015 (2020)

[37] Srinivasan S G, Van Duin A C T, Ganesh P. Development of a ReaxFF potential for carbon condensed phases and its application to the thermal fragmentation of a large fullerene. *J Phys Chem A* **119**(4): 571–580 (2015)

[38] Jensen B D, Wise K E, Odegard G M. Simulation of the elastic and ultimate tensile properties of diamond, graphene, carbon nanotubes, and amorphous carbon using a revised ReaxFF parametrization. *J Phys Chem A* **119**: 9710–9721 (2015)

[39] Xu J, Wang Y, Cen Y, Xing B, Zheng X, Ootani Y, Kubo M, Prediction of macroscopic properties of diamond-like carbon from atomic-scale structure. *J Phys Chem C* **123**: 24609–24614 (2019)

[40] Zheng X, Zhu H, Kosasih B, Tieu A K. A molecular dynamics simulation of boundary lubrication: The effect of n-alkanes chain length and normal load. *Wear* **301**(1–2): 62–69 (2013)

[41] Matta C, De Barros Bouchet M I, Le-Mogne T, Vachet B, Martin J M, Sagawa T. Tribochemistry of tetrahedral hydrogen-free amorphous carbon coatings in the presence of OH-containing lubricants. *Lubr Sci* **20**(2): 137–149 (2008)

Yun LONG. He received his bachelor degree in material physics at 2011 from Northeastern University, Shenyang, China. Then, he pursued master degree of nano engineering at Institut National des Sciences Appliquées, Lyon, France. And he was granted with doctor degree by Ecole Centrale de Lyon, France in 2020. His research interests include fundamental study of superlubricity mechanism and commercial additives development.

Maria Isabel De Barros BOUCHET. She received her doctoral degree on the "Development and characterisation of diamond coatings for tribological applications" from Institut de Combustion, Aérothermique, Réactivité et Environnement (ICARE, CNRS) in France. She joined the Laboratory of Tribology and System Dynamics at Ecole Centrale de Lyon from 2001. She is a lecturer in the Department of Materials and Surface Sciences and deputy director of research of école centrale de Lyon (ECL). Her research activities cover surface science, tribochemistry, and superlubricity mechanisms.